European Journal of Pharmaceutical Sciences 194 (2024) 106702

Contents lists available at ScienceDirect

European Journal of Pharmaceutical Sciences

journal homepage: www.elsevier.com/locate/ejps

Development of a canine artificial colonic mucus model for drug diffusion studies

V. Barmpatsalou [a], M. Tjakra [a], L. Li [a], I.R. Dubbelboer [b], E. Karlsson [c], B. Pedersen Lomstein [d,1], C.A.S. Bergström [a,*]

[a] The Swedish Drug Delivery Center, Department of Pharmacy, Uppsala University, Box 580, SE-751 23, Uppsala, Sweden
[b] The Swedish Drug Delivery Center, Department of Pharmaceutical Biosciences, Uppsala University, Box 574, SE-751 23, Uppsala, Sweden
[c] Oral Product Development, Pharmaceutical Technology & Development, Operations, AstraZeneca, Gothenburg, Sweden
[d] Product Development & Drug Delivery, Global Pharmaceutical R&D, Ferring Pharmaceuticals A/S, Amager Strandvej 405, 2770, Kastrup, Denmark

ARTICLE INFO

Keywords:
Artificial mucus
In vitro
Drug diffusion
Drug permeation
Drug binding
Rheology
Hydrogel

ABSTRACT

Colonic mucus is a key factor in the colonic environment because it may affect drug absorption. Due to the similarity of human and canine gastrointestinal physiology, dogs are an established preclinical species for the assessment of controlled release formulations. Here we report the development of an artificial colonic mucus model to mimic the native canine one. *In vitro* models of the canine colonic environment can provide insights for early stages of drug development and contribute to the implementation of the 3Rs (refinement, reduction, and replacement) of animal usage in the drug development process. Our artificial colonic mucus could predict diffusion trends observed in native mucus and was successfully implemented in microscopic and macroscopic assays to study macromolecular permeation through the mucus. The traditional Transwell set up was optimized with the addition of a nylon filter to ensure homogenous representation of the mucus barrier *in vitro*. In conclusion, the canine artificial colonic mucus can be used to study drug permeation across the mucus and its flexibility allows its use in various set ups depending on the nature of the compound under investigation and equipment availability.

1. Introduction

The gastrointestinal (GI) mucus is a hydrogel covering the surface of the gastrointestinal tract (GIT). It hydrates and lubricates the epithelium (Cone, 2009), shields the epithelial cells from the acidic environment of the stomach, and protects against pathogens in the GI lumen (Taherali et al., 2018; Johansson et al., 2014). Mucus is composed of 90–95 % water. The key building block, the mucins—a class of glycosylated proteins of high molecular weight (MW)—comprise 5 % of the dry weight (Larhed et al., 1998; Bansil and Turner, 2006; Dubbelboer et al., 2022). Mucins can be either membrane-bound or secreted from the goblet cells (Johansson et al., 2013). The MUC5A is the main type of mucin secreted in the stomach, while MUC2 predominates in the intestine. Mucins connect to each other via end-to-end disulfide bonds, and form a larger complex network, which is also mediated by chain entanglements, hydrophobic interactions between the non-glycosylated, cysteine-rich regions, and electrostatic repulsion between the negatively charged polysaccharide sidechains (Johansson et al., 2013; Boegh and Nielsen, 2015; Wagner et al., 2018).

From a drug delivery perspective, the mucus layer is a potential barrier against drug absorption through the GI epithelium after oral administration (Cone, 2009; Taherali et al., 2018; Boegh and Nielsen, 2015). As GI mucus is continuously secreted and shed from the epithelium, drug molecules or particles adhering to the mucus layer might be flushed away before reaching the epithelium (Boegh and Nielsen, 2015). The steric network of mucus can also limit the diffusion of larger drug particles or vehicles (Wagner et al., 2018; Ensign et al., 2013). Lipids and hydrophobic domains of the mucins can interact with lipophilic drugs, resulting in limited diffusion (Larhed et al., 1998; Sigurdsson et al., 2013) and the functional groups (e.g. carboxylic groups) might also bind to drug molecules (Cone, 2009; Bhat et al., 1996). In some disease states, such as inflammatory bowel disease (IBD) (Johansson et al., 2013; Etienne-Mesmin et al., 2019) the composition and structure of the mucus layer can be altered. Therefore, it is of great value to understand

* Corresponding author.
E-mail address: christel.bergstrom@farmaci.uu.se (C.A.S. Bergström).
[1] current affiliation: Oral Solids Development, Janssen R&D, Johnson & Johnson, Turnhoutseweg 30, B-2340, Beerse, Belgium

https://doi.org/10.1016/j.ejps.2024.106702
Received 27 September 2023; Received in revised form 14 December 2023; Accepted 7 January 2024
Available online 12 January 2024

the impact of GI mucus on drug absorption, in both healthy and disease states.

In preclinical stages of drug discovery and development, dogs are often used for the assessment of controlled release (CR) or modified release (MR) formulations, due to their similarities in physiology to humans (Sutton, 2004; Sjögren et al., 2014). The size of the dog enables the administration of dosage forms intended for subsequent clinical stages (Dressman, 1986; Dahlgren et al., 2016), and similarities in motility patterns and pH profiles between dogs and humans (Dahlgren et al., 2016) allow development of rational methods to predict the drug behavior in humans (Akimoto et al., 2000). For example, Sutton et al. developed a colonoscopy model for predicting human colonic absorption, using Beagle dogs. The model predicted colonic permeability reasonably well with a correlation (R^2) of 0.8 between dogs and humans when comparing the relative bioavailability of a series of model compounds (propranolol, aminophylline, enalapril, nifedipine, azithromycin, sertraline and trovafloxacin) in solution. They proposed that the model could be a surrogate for human intubation studies when the CR candidates belong to Biopharmaceutics Classification System (BCS) classes II, III and IV (Sutton et al., 2006).

In the same direction, a colonoscopic method was developed by Tajiri et al. to evaluate the colonic absorption of extended-release (ER) solid formulations. The absorption profiles of diclofenac, morphine and felodipine solutions were administered to Beagle dogs to compare the bioavailability of the ER formulations to references in humans (Tajiri et al., 2010). A study from Dahlgren et al. determined the regional intestinal effective permeability (P_{eff}) of four model drugs (atenolol, enalaprilat, metoprolol and ketoprofen) in jejunum and colon in Labrador dogs. Jejunal P_{eff} values correlated highly to human data (R^2 = 0.98) from a previous study. Dog P_{eff} values were also successfully implemented in *in silico* models to predict human absorption (Dahlgren et al., 2016). A study from Wu et al. demonstrated that the Beagle dog is a good model for the evaluation of nanoparticle formulations, correlating well with human PK data (Wu et al., 2004).

Although *in vivo* studies in dogs remain the gold standard to assess the bioavailability of MR formulations in the preclinical stage, they are increasingly restricted by regulations, ethical constraints, and high costs (Deschamps et al., 2022). The 3R principles (replace, reduce and refine), originated by Russell and Burch in 1959, encourage the reduction of animal use in research, to minimize animal pain and distress (Tannenbaum and Bennett, 2015). Additionally, a high degree of interanimal variability is common, an aspect that lowers the reproducibility of the assays and hinders interpretation of the results (Wagner et al., 2018; Deschamps et al., 2022; Lock et al., 2018). Therefore *in vitro* models with high biorelevance are a useful alternative in the early stages of formulation screening: They offer higher flexibility, reproducibility, and lower cost.

To increase the physiological relevance of *in vitro* models, various approaches have used native mucus, artificial purified mucus, mucus-secreting cell cultures, and mucosal tissue (Lock et al., 2018; Berben et al., 2018; Fedi et al., 2021). Although the mucus of animal origin preserves the original composition and structural characteristics, collecting and handling it is complex, especially in larger animals like pigs and dogs (Dubbelboer et al., 2022; Barmpatsalou et al., 2021). Cell cultures with mucus-secreting function, such as the co-culture model Caco-2/HT-29 (Wikman-Larhed and Artursson, 1995), is an alternative to represent the mucus barrier. However, the secreted mucus may not match the structure and adhesive characteristics of native mucus; it forms patches only on top of the HT29 cells rather than an evenly distributed layer on the monolayer (Béduneau et al., 2014; Xavier et al., 2019). Artificial mucus would therefore be advantageous in the early stages of drug discovery and development, due to a well-defined composition and homogeneity, easier preparation, and lower batch-to-batch variations (Lock et al., 2018).

Although it has been reported that solutions of purified mucin do not have the same rheological properties as native mucus, adding polymers can increase the cross-linking of the gel network (Kocevar-Nared et al., 1997; Boegh et al., 2014). Boegh et al. developed a biosimilar mucus mimicking the porcine jejunal mucus by using purified gastric mucin, lipids, albumin and an anionic polymer, polyacrylic acid (PAA, Carbopol 974P NF). The biosimilar mucus shows properties and microstructure comparable to porcine small intestinal mucus. Biosimilar mucus coupled with Caco-2 cells showed lower permeated amount of both hydrophilic and lipophilic model drugs, compared to Caco-2 cells layer alone, indicating the barrier properties of the mucus (Boegh et al., 2014).

Deschamps et al. recently compiled an overview of *in vitro* models simulating the canine GIT (Deschamps et al., 2022). Most of them were used for nutritional applications, with a focus on digestion. Only one incorporated a colonic mucus feature, in the form of a mucin-agar mixture (Verstrepen et al., 2021). There were also a few studies focusing on canine gastric mucus (Zalewsky et al., 1983; Zalewsky and Moody, 1979) but information about the canine colonic mucus in the literature remains limited. As gastric and colonic canine mucus have different characteristics (Dubbelboer et al., 2022), it is essential to develop a canine colonic model with a physiologically relevant artificial mucus. A relevant model is a critical factor for proper study of controlled/delayed/sustained drug release or colonic drug delivery.

The aim of the present study was two-fold: The first goal was to develop a canine artificial colonic mucus model based on multi-omics analyses and the structural profiling of canine native colonic mucus reported by Dubbelboer et al. (Dubbelboer et al., 2022). The second goal was to explore the versatility of the artificial mucus model in reflecting variations of mucus viscosity in disease states and the implementation of the artificial mucus model in microscopic and macroscopic permeation assays to study the impact of mucus on macromolecular diffusion.

2. Methods

2.1. Materials

Fluorescein isothiocyanate (FITC)–diethylaminoethyl (DEAE)–dextran (cationic) with molecular weight of 4 kDa, FITC–carboxymethyl (CM)–dextrans (anionic) with molecular weights of 4 and 40 kDa and non-ionic FITC–dextrans with molecular weights of 4, 40 and 70 kDa were purchased from Sigma Aldrich (St. Louis, MO, USA). Corning Costar Snapwell cell culture 12-mm inserts and 0.4-μm pore polycarbonate membranes in 6-well plates, 2-(N-morpholino)ethanesulfonic acid (MES), polysorbate 80 (Tween 80), $CaCl_2$, $MgSO_4$, cholesterol, mucin from porcine stomach Type II and Type III, bovine serum albumin (BSA) were also obtained from Sigma Aldrich. The two Types of mucin from porcine stomach undergo different purification treatments.

Phosphatidylcholine (PC, 98 %) was provided by Lipoid (Ludwigshafen, Germany). Polyacrylic acid (PAA; Carbopol 974P NF) was acquired from Lubrizol (Brussels, Belgium) and NaCl from Merck Chemicals (Darmstadt, Germany). The nylon net filter (11-μm pore size) was purchased from Merck Millipore (Billerica, MA, US) and acetonitrile (LC grade) was purchased from VWR.

2.2. Collection of canine native colonic mucus

Canine native colonic mucus was collected as described previously (Dubbelboer et al., 2022). Briefly, tissue samples of the proximal colon of two male, non-castrated Labradors were obtained from AstraZeneca (Mölndal, Sweden), after euthanasia. One dog (DZ02) was 5 years of age and 35.9 kg; the other (DZ04) was 7 years old and 37.9 kg. Both dogs belonged to a research colony and were euthanized for reasons other than this study, so no additional ethical permit was required for the present investigation. Neither dog suffered from GIT-related diseases, had undergone any invasive GIT treatment/ surgery/endoscopy/colonoscopies, or had vomiting or diarrhea within the final month. Both dogs had permanent nipple-valve stomas surgically inserted into the duodenal, jejunal, or proximal colonic abdominal wall.

After excision, the tissues were stored in ice-cold Krebs Ringers buffer (pH 7.3) and kept on ice for 6 h until the mucus collection. The colonic tissue from both dogs was rinsed with cold buffer (10 mM MES isotonic buffer containing 1.3 mM $CaCl_2$, 1.0 mM $MgSO_4$, and 137 mM NaCl, pH 6.5), and mucus collection was performed as previously described (Dubbelboer et al., 2022). The mucus samples were aliquoted within 5 h after collection, snap-frozen in liquid nitrogen immediately thereafter, and stored at −80 °C until further analyses.

2.3. Preparation of canine artificial colonic mucus

Preparation of the canine artificial colonic mucus (CACM) samples was based on the characterization of proximal colonic mucus of canine origin in previous studies (Dubbelboer et al., 2022) and on protocols proposed by Boegh et al. (Boegh et al., 2014). CACM contained 2.67 % (w/v) mucin Type II ($CACM_{II}$) or III ($CACM_{III}$), 12.08 % (w/v) BSA, 1 % (v/v) lipid mixture (0.12 % cholesterol and 0.14 % phosphatidylcholine, mixed with Tween 80 in a 3:1 lipid:Tween 80 ratio) and 0–1.8 % (w/v) PAA. The lipid mixture was prepared by dissolving the lipids in isotonic buffer (10 mM MES with 1.3 mM $CaCl_2$, 1.0 mM $MgSO_4$, and 137 mM NaCl, pH 6.5) in the presence of Tween 80 under intense stirring.

PAA was transferred in 9 ml of a non-isotonic buffer (10 mM MES with 1.3 mM $CaCl_2$, 1.0 mM $MgSO_4$, pH 6.5) and then mucin Type II or III was added. The mixture was vigorously vortexed, followed by the addition of 120 µl of 5 M NaOH and BSA. The resulting mixture was vortexed again until no solids were visible by eye, after which the lipid mixture was added and the pH adjusted to 6.5 by dropwise addition of 5 M NaOH. The mixture was stored overnight at 4 °C and the next day the sample was transferred to −80 °C until further analyses.

2.4. Zeta potential measurements

Native colonic mucus (50 mg) from DZ02 and DZ04, $CACM_{II}$ and $CACM_{III}$ samples were dissolved in 10 ml deionized water under magnetic stirring and a portion of the mixture was used to fill an Omega cuvette. The zeta potential was measured with a DLS Litesizer 500 (Anton Paar, Austria), after a 1-min equilibration at 25 °C. The results were processed with the instrument's Kalliope software, version 2.8.3.

2.5. Rheological measurements

The artificial mucus samples were thawed at room temperature for the rheological measurements. An ARES-G2 strain-controlled rheometer (TA Instruments, Sollentuna, Sweden) with the Advanced Peltier System (APS) accessory for the lower plate was used. The lower geometry was a 60-mm diameter, APS quick-change flat plate from hardened chromium and the upper geometry was a 40-mm stainless steel cone plate (0.0175 rad). The apparent viscosity of the CACM samples was measured at 37 °C under increasing shear rates, ranging from 1 to 100 s^{-1}. The viscoelastic properties of the CACM samples were measured from frequency sweeps (range 0.63–20 rad/s at 1 % oscillation strain), at 37 °C. The selection of 1 % oscillation strain was based on the linear viscoelastic region (LVR). The LVR was determined with an amplitude sweep, during which the oscillation strain was increased from 0.1 to 100 % at a frequency of 1 Hz oscillation. The 1 % oscillation strain was within the LVR, ensuring nondestructive measurements for the samples.

2.6. Cryo scanning electron microscopy and image analysis

Cryo scanning electron microscopy (CryoSEM) was performed by the Umeå centre for Electron Microscopy (UCEM) as previously described (Dubbelboer et al., 2022) and was used to elucidate the mucus network. In brief, the mucus samples were thawed at room temperature and a single drop was cast onto a metal holder. The sample was vitrified in liquid nitrogen and upon freezing, fractured with a cold knife, and sublimated in vacuum at −90 °C for 30 min. The imaging of the mucus network was performed using a Carl Zeiss Merlin field-emission cryogenic scanning electron microscope, fitted with a Quorum Technologies PP3000T cryo preparation system. Images were acquired at −140 °C by an in-chamber secondary electron detector at an accelerating voltage of 2 kV and a probe current of 50 pA. Selected CryoSEM images of suitable quality for image analysis were appropriately thresholded, transformed to binary form, and mucus pores were identified by ImageJ software (version 1.52a, National Institutes of Health, USA). The pores were characterized in terms of size and shape. Feret's minimum diameter—defined as the shortest distance between any two parallel tangents of a pore—was used as pore size descriptor and the Aspect Ratio (AR), which is the ratio of Feret's max (F_{max}) diameter to Feret's min (F_{min}) diameter, was used as pore shape descriptor (Eq. (1)).

$$AR = \frac{Fmax}{Fmin} \quad \text{(Eq. 1)}$$

2.7. Fluorescence recovery after photobleaching

The diffusion of FITC-dextrans in canine native and artificial colonic mucus was assessed by fluorescence recovery after photobleaching (FRAP), using a Zeiss CLSM 780 and the data were collected with the ZEN Black software (Carl Zeiss GmbH, Jena, Germany). Experiments with FITC-dextrans of various charges and sizes (4 and 40 kDa MW for anionic FITC–dextrans, 4 kDa MW for the cationic and 4, 40 and 70 kDa MW for the non-ionic ones) were conducted as previously described (Barmpatsalou et al., 2023) to elucidate the impact of charge and molecular weight on diffusion.

The diffusivity values were calculated as previously described (Brandl et al., 2010). Briefly, the fluorescence intensities of the bleached region of interest (ROI) and a reference ROI were initially normalized to the pre-bleach intensity and a least squares fit was performed on the recovery curve (Eq. (2)) in R (code available upon request) to determine the characteristic diffusion time τ_D.

$$F(t) = k \cdot e^{-\frac{\tau D}{2t}} \left[Io\left(\frac{\tau D}{2t}\right) + \mathrm{I}_1\left(\frac{\tau D}{2t}\right) \right] \quad \text{(Eq. 2)}$$

where I_0 and I_1 are the zero and first order modified Bessel functions of the first kind and k corresponds to the mobile fraction. Finally, the diffusivity values were obtained by solving $D = w^2/\tau_D$, where w is the radius of the bleached ROI (16 µm). Three FRAP measurements were made for each sample.

2.8. Permeability assay

The permeability studies were conducted in 6-well Snapwell plates (insert filter diameter 12 mm). CACM samples (200 mg) were added to the filters and equilibrated for 10 min under continuous shaking to obtain a homogenous mucus layer. Thereafter, circular nylon filters (diameter 12 mm) were carefully placed on top of the mucus, to ensure the layer remained intact after introduction of the donor solution to the mucus-containing insert. Hanks' balanced salt solution (HBSS) (2 ml, pH 7.4), supplemented with 0.05 % BSA, was added to the receiver compartment. The experiment was initiated by slowly adding 300 µl of FITC-dextran donor solution (250 µg/ml, in HBSS (pH 7.4)) on top of the nylon filter inserts to avoid creating holes in the hydrogel. The plates were incubated in an orbital shaker at 100 rpm, 37 °C for 3 h. Samples (400 µl) were collected from the basolateral side of each filter at predefined time intervals, and the volume was replenished by the same amount of fresh HBSS buffer (at 37 °C). Only concentrations above the lower limit of quantification (LOQ)—which was determined to be three times the signal of the blank—were included in the calculations. Fresh calibration curves were prepared with serial dilutions in the range of 0.002–78 µg/ml. The samples and calibration curve were transferred to a 96-well black plate (TECAN Austria), diluted 1:1 with acetonitrile to precipitate the BSA, and were centrifuged at 1370 *g* at 5 °C for 10 min.

The fluorescent signal of the FITC-dextran was measured at λ_{ex} 485 nm and λ_{em} 520 nm in a TECAN SPARK Microplate Reader (TECAN Austria).

The amount (%) of FITC-dextrans that diffused through the mucus layer was calculated based on the total amount of FITC-dextran transferred to the basolateral side in relation to the initial amount of FITC-dextran that was added in the apical side of the filters. The mass balance was determined based on the amount of FITC-dextran that could be detected in the apical and the basolateral side upon experimental completion compared to the amount of FITC-dextran that was added in the apical side of the filters upon experimental initiation.

2.9. Microscale thermophoresis (MST)

The interaction between FITC-dextrans and CACM was studied using the MST imaging device (Monolith NT.Automated) with capillary chips from NanoTemper Technologies GmbH (Germany). Stabile temperature

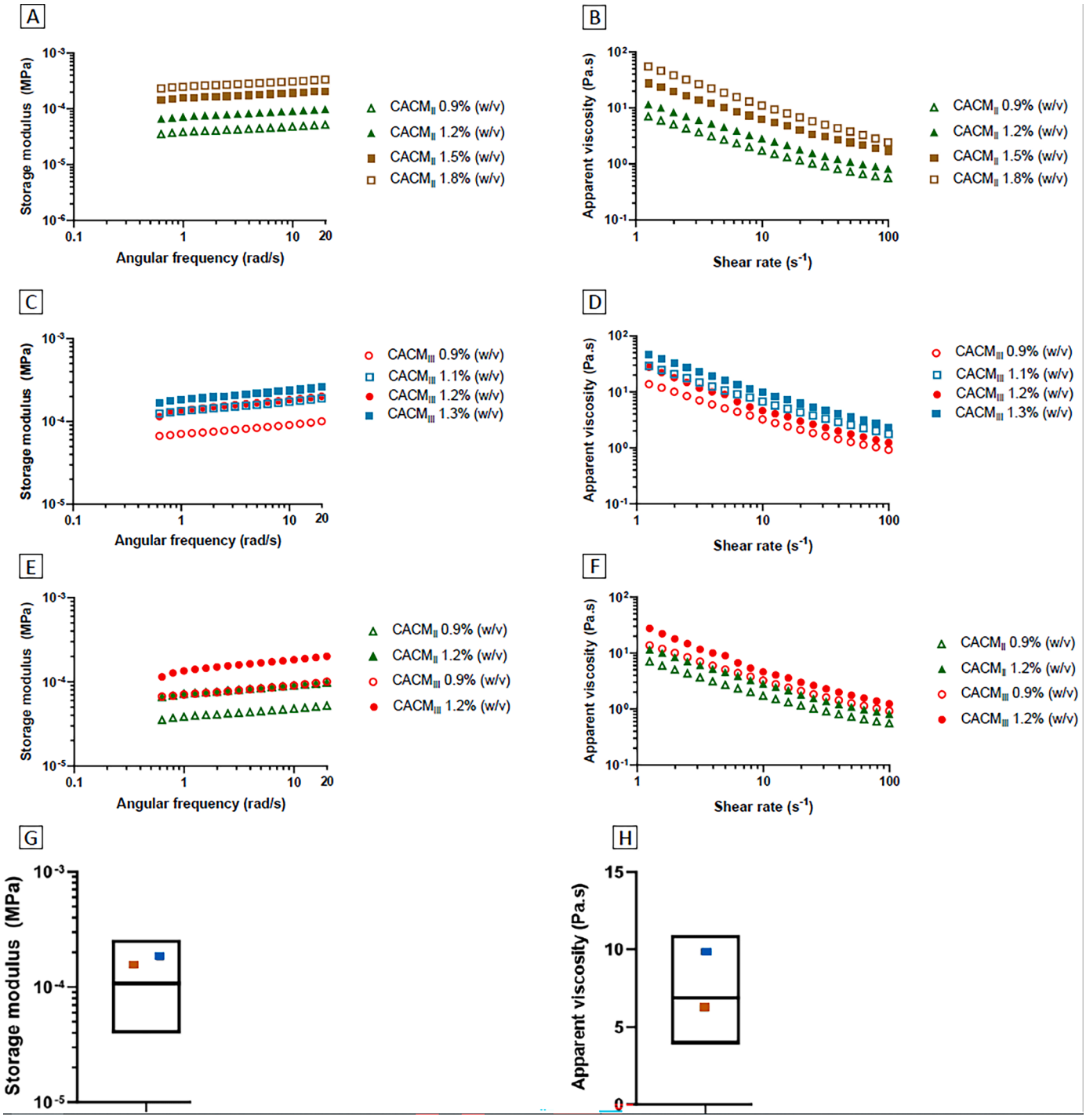

Fig. 1. Rheological profiling of CACM$_{II}$ and CACM$_{III}$. Effect of increasing amounts of PAA in the storage modulus and apparent viscosity of CACM$_{II}$ (A, B) and CACM$_{III}$ (C, D) samples. Comparison between the storage modulus (E) and apparent viscosity (F) profiles of CACM$_{II}$ and CACM$_{III}$ samples containing equal amounts of PAA. Comparison between the storage modulus values at 1 rad/s (G) and apparent viscosity at 10 s^{-1} (H) of CACM$_{II}$ (brown squares) and CACM$_{III}$ (blue squares) as well as canine native colonic mucus from a previous study (Dubbelboer et al., 2022). Floating bars depict the range; the line depicts the mean of canine native colonic mucus data.

of 25 °C was maintained for all experiments and fluorescence levels of FITC-dextrans and CACM at designated capillary positions were recorded. FITC-dextrans of various charge and size properties were used (see Materials section) as ligands, after being dissolved in 10 mM MES buffer pH 6.5. A pretest step was performed to determine the detectable concentrations of FITC-dextran using a Nano-Blue detector with λ_{ex} 495 nm and λ_{em} 519 nm following the recommended settings for FITC. Concentrations of 2000 nM, 400 nM, and 200 nM were selected for the 4 K, 40 K, and 70 K dextrans, respectively. Freshly prepared CACM was dispersed in 10 mM MES buffer as the stock solution (5 mg/mL) and the targets were prepared by serial dilutions of the CACM stock solution with 10 mM MES buffer containing 0.3 % Tween-20 (resulting concentrations in the range of 0.0024- 5 mg/mL) to prevent adsorption of the samples to the capillary chips. Mixtures of ligands and targets were inserted into capillary chips followed by readings with 10 % excitation power and low MST power for 3 s pre-MST, 10 s during MST, and 1 s post-MST. All buffers and samples were properly degassed by sonication prior to the experiments. All experiments were performed in triplicate. Following the experiments, the normalized fluorescence was plotted as a function of concentration of the target to determine the dissociation constant (K_d). The K_d indicates the equilibrium between ligand-target complex and describes the concentration dependent binding interaction. Reports and analysis of K_d-fit were generated using MO.Affinity Analysis (NanoTemper, Germany) software.

2.10. Data visualization-Statistics

GraphPad Prism (GraphPad Software, CA, USA) was used for data visualization and statistical analyses. Unpaired *t*-test was used to evaluate differences between two groups, while a one-way ANOVA, followed by Holm-Sidak's multiple comparisons test was used to evaluate differences between more than two groups. P values less than 0.05 were considered statistically significant.

3. Results

3.1. Rheological comparison

CACM was developed based on the composition of canine native colonic mucus as reported in previous investigations (Dubbelboer et al., 2022). Initial preparations of $CACM_{II}$ and $CACM_{III}$ did not have gel-like characteristics and thus polyacrylic acid (PAA) was added to them to increase the viscosity and cross-linking of the samples, as done previously (Boegh et al., 2014).

Fig. 1A-D depicts the storage modulus and apparent viscosity profiles of $CACM_{II}$ and $CACM_{III}$ samples with increasing PAA concentrations. As illustrated in Fig. 1E and F, the addition of equal amounts of PAA to the $CACM_{II}$ and $CACM_{III}$ samples resulted in higher storage modulus and apparent viscosity values for the $CACM_{III}$. $CACM_{II}$ samples with 1.5 % (w/v) PAA and $CACM_{III}$ samples with 1.3 % (w/v) PAA reflected the rheological profile of canine native colonic mucus, (Fig. 1G and H), and were thus selected for further analyses.

3.2. Comparison based on gel network microarchitecture

The mucus network microarchitecture of 0, 0.9, and 1.5 % (w/v) PAA $CACM_{II}$ and 0, 0.9, and 1.3 % (w/v) PAA $CACM_{III}$ samples was visualized with CryoSEM, with the same microscopy conditions used previously to characterize canine native colonic mucus (Dubbelboer et al., 2022). Neither $CACM_{II}$ nor $CACM_{III}$ showed gel-like characteristics in the absence of PAA; however, the micrographs revealed that "loose" structures could be formed (Fig. 2A and B). The addition of PAA resulted in the gradual adaptation of a "honeycomb" structure (Fig. 2A-F), which resembled the structural characteristics of canine native colonic mucus (Fig. 2G). Both $CACM_{II}$ and $CACM_{III}$ samples formed extensive pore networks which were highly homogenous, as outlined in micrographs at lower magnification (Fig. 2H and I). Image analysis (Fig. 2J) confirmed that the addition of PAA resulted in a pore network with significantly lower mean Feret's minimum diameter and AR for $CACM_{II}$. For $CACM_{III}$ samples, PAA decreased the mean Feret's minimum diameter and did not affect the AR values (Fig. 2K).

3.3. Zeta potential measurements

The zeta potential values of native and artificial colonic mucus are presented in Table 1. All mucus samples had negative zeta potential. Native colonic mucus from the two dogs, DZ02 and DZ04, had similar zeta potential values to each other, and were higher than the values for artificial colonic mucus models $CACM_{II}$ and $CACM_{III}$.

3.4. Diffusivity measurements

3.4.1. Diffusion of FITC-dextrans in canine native colonic mucus

The diffusion of FITC-dextrans in canine native colonic mucus was monitored by FRAP. Fig. 3A shows the diffusivity values of FITC-dextrans in canine native colonic mucus samples from the two laboratory dogs (DZ02 and DZ04). There was a trend towards lower diffusivity values of the FITC-dextrans in DZ02, compared to DZ04. For both dogs, the diffusion of cationic 4 K FITC-dextran was significantly lower compared to that of either anionic or neutral 4 K FITC-dextrans. For DZ02, there was no significant difference between the diffusivity values of 4 K and anionic 4 K FITC-dextrans (Fig. 3B); however, for DZ04 these values were significantly different (Fig. 3C). No significant differences were observed between the diffusivity values of FITC-dextrans 40 K and anionic 40 K in colonic mucus samples from the two dogs. In both animals, the diffusivity values of 4 K FITC-dextran were significantly higher compared to those of 40 K and 70 K (Fig. 3B and C).

3.4.2. Comparison based on diffusion of FITC-dextrans

The rheological properties of the $CACM_{II}$ samples with 1.5 % (w/v) PAA and $CACM_{III}$ with 1.3 % (w/v) PAA were similar to the ones of canine native colonic mucus. However, $CACM_{II}$ was selected as the CACM representative for the further analyses, because it was less cumbersome to prepare than $CACM_{III}$ (intensive vortexing was required to dissolve the solids) and because the mucin Type III is more expensive. CACM was compared to canine native colonic mucus in terms of the diffusion profiles of FITC-dextrans of various charges and sizes. Fig. 4A and B show the diffusivity values of the various FITC-dextrans in canine native colonic mucus from DZ02, DZ04 and CACM. In all cases, the diffusivity values of FITC-dextrans from CACM samples were not significantly different compared to the canine native colonic mucus from DZ02. However, they were significantly different compared to DZ04, with the exception of 70 K FITC-dextran (Fig. 4A and B).

3.5. Permeability studies

3.5.1. Impact of altered viscosity on the diffusion of FITC-dextrans in canine artificial colonic mucus

The impact of altered viscosity of the CACM samples on the diffusion of FITC-dextrans was studied by introducing CACM samples with 0.6 % and 1.8 % (w/v) PAA (representing lower and higher viscosity values compared to reference $CACM_{II}$, respectively) to the permeability set up. The rheological profiles of the CACM sample containing 0.6 % (w/v) PAA, referred to as L-CACM and the CACM sample containing 1.8 % (w/v) PAA, referred to as H-CACM, are shown in Fig S1. Fig. 5 illustrates the fold difference of the permeated amount (%) of FITC-dextrans through L-CACM and H-CACM, compared to the reference CACM. Permeation was higher for all of the FITC-dextrans in L-CACM compared to CACM, but the differences were not significant, except for the 4 K (Fig. S2). The permeated amount of FITC-dextrans through H-CACM was similar to CACM. For all three CACMs, there was a trend towards less permeation of the cationic 4 K FITC-dextran compared to the neutral and anionic

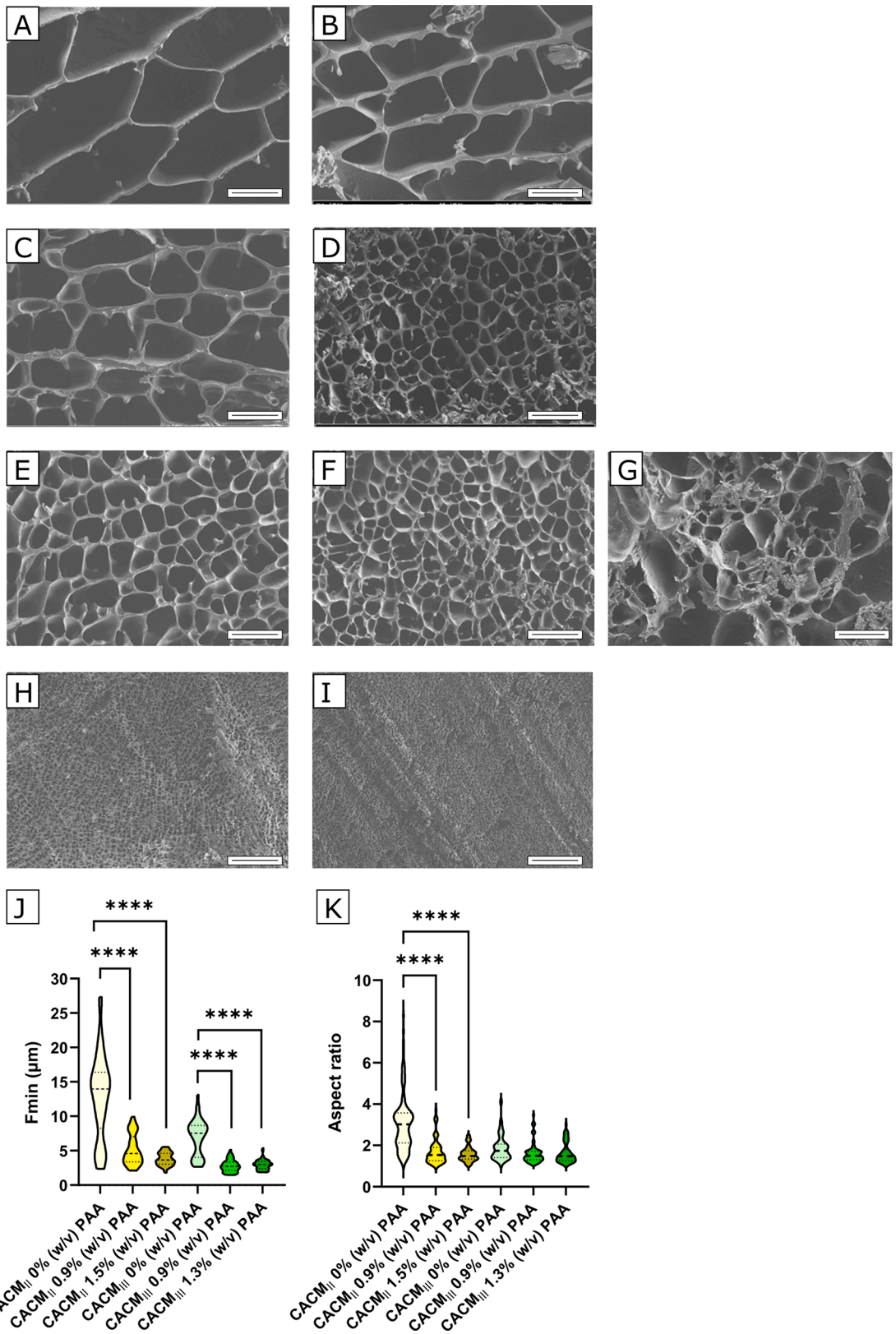

Fig. 2. Structural comparison of $CACM_{II}$ and $CACM_{III}$: Representative cryo-scanning electron micrographs at 5000X magnification of: $CACM_{II}$ (A) and $CACM_{III}$ (B) without PAA; $CACM_{II}$ (C) and $CACM_{III}$ (D) with 0.9 % (w/v) PAA; $CACM_{II}$ with 1.5 % (w/v) PAA (E); $CACM_{III}$ with 1.3 % (w/v) PAA (F); and canine native colonic mucus (G). Scale bars: 10 μm. Representative cryo-scanning electron micrographs of $CACM_{II}$ (H) and $CACM_{III}$ (I) at 500X magnification. Scale bars: 100 μm. Violin plots of Feret's minimum diameter (J) and aspect ratio distribution (K) comparing $CACM_{II}$ and $CACM_{III}$ samples, with increasing amount of PAA. Dotted lines represent the 25 % and 75 % percentiles, while the dashed line represents the median. Approximately 50 pores per sample were identified and used in the analysis.

Table 1
Zeta potential measurements of native colonic mucus from dogs DZ02 and DZ04 and artificial colonic mucus ($CACM_{II}$ and $CACM_{III}$).

	Mean	SD	n
$CACM_{II}$	−41.9	2.5	5
$CACM_{III}$	−44.0	2.2	5
DZ02	−31.6	0.5	3
DZ04	−32.6	0.8	3

ones. The negative charge apparently did not affect the amount of 4 K and 40 K dextrans permeating through any of the CACMs studied. Furthermore, FITC-dextrans of higher MW (40 K and 70 K) permeated less through CACM, L-CACM and H-CACM (Fig. S2) than the 4 K FITC-dextran. The calculated mean mass balance was 80 % in all experiments, with the exception of the cationic 4 K FITC-dextran (55 %). We speculate that strong binding between the cation and the negatively charged mucins resulted in retainment of the FITC-dextran leading to incomplete quantification of the remaining cationic 4 K FITC-dextran in the donor compartment.

3.5.2. *Impact of mucus components on the diffusion of FITC-dextrans in canine artificial colonic mucus*

The impact of mucus components (mucin, BSA, and lipids) was monitored by measuring the permeation of FITC-dextrans through the CACM samples. Samples were prepared with either no mucin, no BSA or no lipids. The permeation of 4 K FITC-dextran was significantly impacted by all three components (Fig. 6A). In their absence, the permeated amount was several fold and significantly higher (Fig. S3). Without mucin, the mean permeated amount of charged 4 K FITC-dextrans (both cation and anion) was almost three-fold and significantly higher, whereas the absence of lipids had no effect (see Fig. 6A and S3). For the FITC-dextrans of higher MW (40 K and 70 K), the

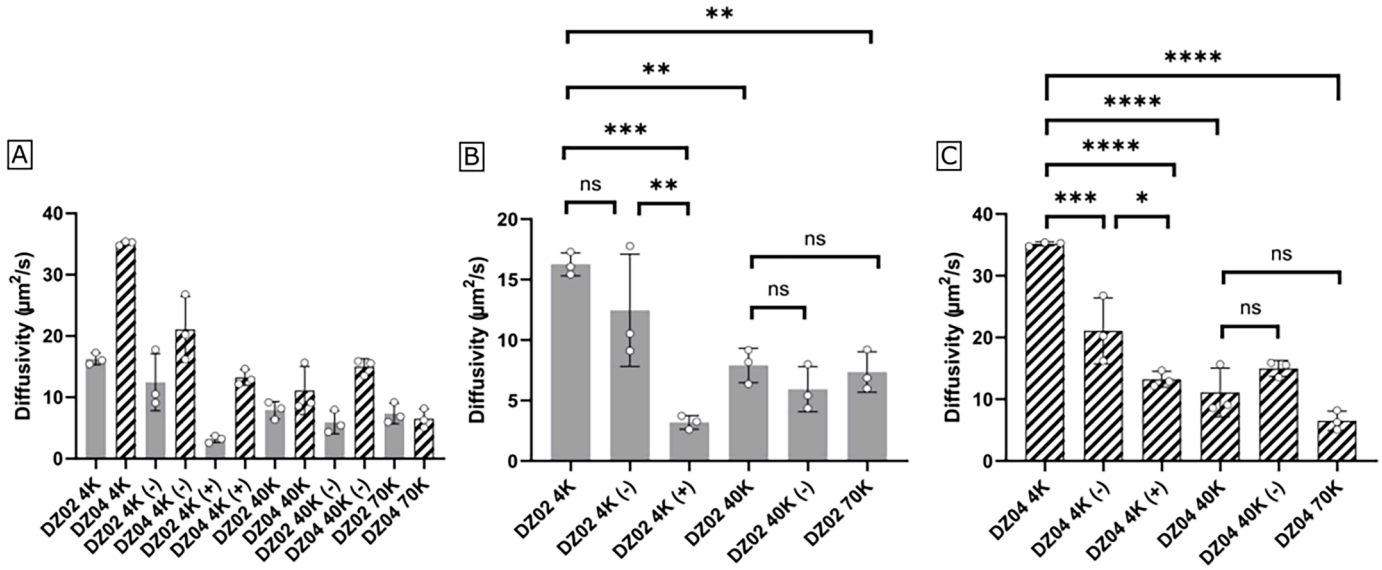

Fig. 3. Comparison of diffusivity values of FITC-dextrans in canine native colonic mucus. Two dogs (DZ02, in gray bars and DZ04, in black stripped bars) were studied (A). Individual profiles and statistical analysis of diffusivity values of FITC-dextrans in colonic mucus from DZ02 (B) and DZ04 (C), $n = 3$. Open circles represent individual measurements. Bars: Means±SD (* $p < 0.05$, ** $p < 0.01$, *** $p < 0.001$, **** $p < 0.0001$, ns: no significance).

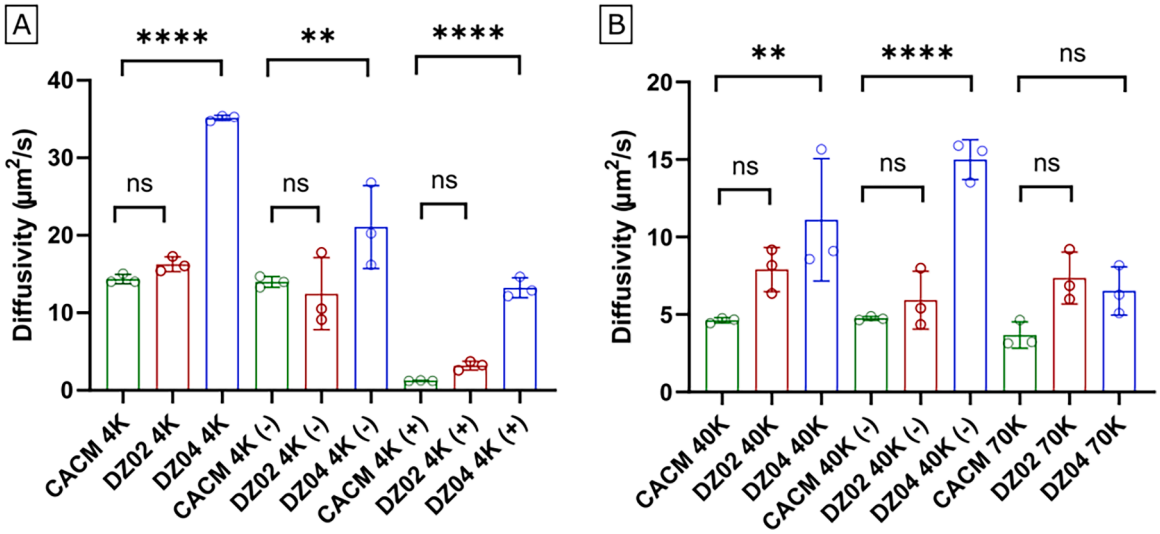

Fig. 4. Diffusivity of FITC-dextrans in native and artificial canine mucus. Comparison of diffusivity values in canine native colonic mucus from two dogs and CACM of 4 K molecular weight FITC-dextrans of different charges (A). Similar profiles for 40 K and 70 K FITC-dextrans (B). CACM (green), dog DZ02 (red) and dog DZ04 (blue). Open circles represent individual measurements. $n = 3$, Bars: Mean±SD (** $p < 0.01$, **** $p < 0.0001$, ns: no significance).

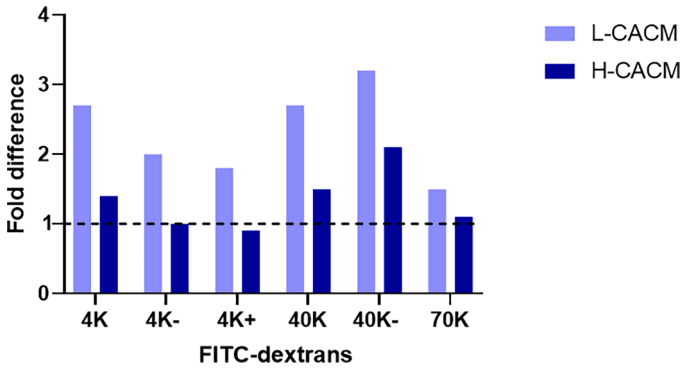

Fig. 5. Comparison of diffusion in low and high viscosity CACMs. Fold difference of mean permeated amount (%) of FITC-dextrans in L-CACM (low viscosity) and H-CACM (high viscosity) with respect to values for CACM reference samples. The dotted line represents the reference CACM baseline.

absence of mucin resulted in an almost 8-fold and significantly higher mean permeated amount, except for the negatively charged ones (Fig. 6B and S3). For 40 K FITC-dextran, the absence of BSA resulted in an almost 10-fold and significantly higher permeated amount.

3.6. Binding studies with MST

The binding between diluted CACM and FITC-dextrans was studied with MST and is presented in Fig. 7A-B. Fig. 7A shows the concentration-dependent interaction between CACM and FITC-dextrans of various charge and size properties. The change in normalized fluorescence was observed only for the cationic 4 K FITC-dextran, while no change was detected for the other FITC-dextrans. Binding interaction would yield different fluorescence intensity levels between the serial dilution of CACM with same amount of FITC-dextrans. The data indicate binding interaction only present between the cationic 4 K FITC-dextran and CACM (Fig. 7B).

Following the measurement, the quality of the data was evaluated by examining the capillary shape chart (Fig. S4). The graph of fitted K_d showed that only the K_d-fit of the cationic 4 K FITC-dextran is successfully plotted by the MO.Affinity Analysis software, while the rest of K_d plots have low confidence level and can be deemed not appropriate for further analysis (Table S1). A detailed illustration of how binding effects are identified in MST experiments is given in Fig. S5A, where a distinct difference in relative fluorescence intensity level is identified for each set of replicates.

4. Discussion

Both $CACM_{II}$ and $CACM_{III}$ initial preparations (containing no PAA) did not present gel-like properties, as already reported for porcine artificial mucus models (Barmpatsalou et al., 2021; Boegh et al., 2014). Neither mucin Type II or III form gels, even at low pH values, probably due to the purification process that commercial mucins undergo, an observation well reported in the literature (Kocevar-Nared et al., 1997; Marczynski et al., 2021). Purification results in substantial loss of functional groups on the commercially available mucins and could be responsible for the limited gelling ability (Marczynski et al., 2021). Due to its mucoadhesive properties, PAA can interact with the mucins via hydrogen bonding (Patel et al., 2003) and can be added to restore the rheological properties of the mucin and form mucus-mimetic gels (Røn et al., 2017).

The addition of PAA resulted in concentration-dependent, gel-like properties for both $CACM_{II}$ and $CACM_{III}$. The gelation was not proportional to the amount of PAA (Fig. 1A-D). This non-proportional increase in apparent viscosity—for both mucin alone (Falavigna et al., 2018) and mucin-PAA solutions (Lefrançois et al., 2015), suggests that both components contribute to the non-linearity.

$CACM_{III}$ samples exhibited higher storage modulus and apparent viscosity values compared to $CACM_{II}$ with equal amounts of PAA. This phenomenon has been observed for mucin Type II and III solutions at pH 7 (Marczynski et al., 2021) and could be related to the levels of ions present in them as the two Types undergo different purification treatments. Ions play a key role in the rheological synergism between PAA and mucin mixtures (Rossi et al., 1995). However, as investigated by Marczynski et al. (Marczynski et al., 2021), there are additional composition differences between mucin Types II and III, which could be affecting their rheological profiles (Fig. 1E and F).

The gel network of $CACM_{II}$ and $CACM_{III}$ was visualized to assess the microarchitecture and compare it to Cryo-SEM images of canine native colonic mucus (Dubbelboer et al., 2022). In the absence of PAA, both $CACM_{II}$ and $CACM_{III}$, presented a "loose network" (Fig. 2A and B; also previously described (Barmpatsalou et al., 2023)). The gradual addition of PAA resulted in the formation of significantly smaller, and more circular, pores in both $CACM_{II}$ and $CACM_{III}$ (Fig. 2J and K). The gradual adaptation of a "honeycomb" structure in PAA gels with increasing amounts of PAA has been previously reported (Kim et al., 2003), and it was evident that addition of PAA in $CACM_{II}$ and $CACM_{III}$,—at comparable amounts—resulted in a denser pore network for $CACM_{III}$ than $CACM_{II}$ (Fig. 2C and D; see also the image analysis, Fig. 2J and K). This phenomenon could be related to the different purification processes that mucin Type II and Type III undergo and which affects the functional groups of the mucins (Marczynski et al., 2021). As already

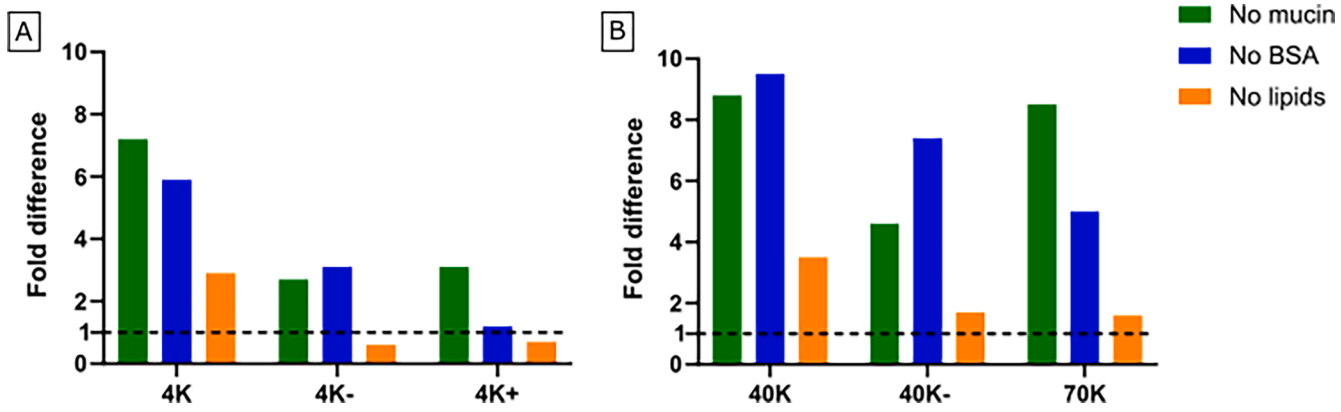

Fig. 6. Impact of components in the artificial mucus on diffusivity. The difference in mean permeated amount of FITC-dextrans in CACM is shown: without mucin (green), without BSA (blue) or without lipids (orange) for 4 K FITC-dextrans (A) and 40 K and 70 K (B). n: 3–6. The dotted line represents the CACM baseline containing all three components (mucin, BSA, lipids).

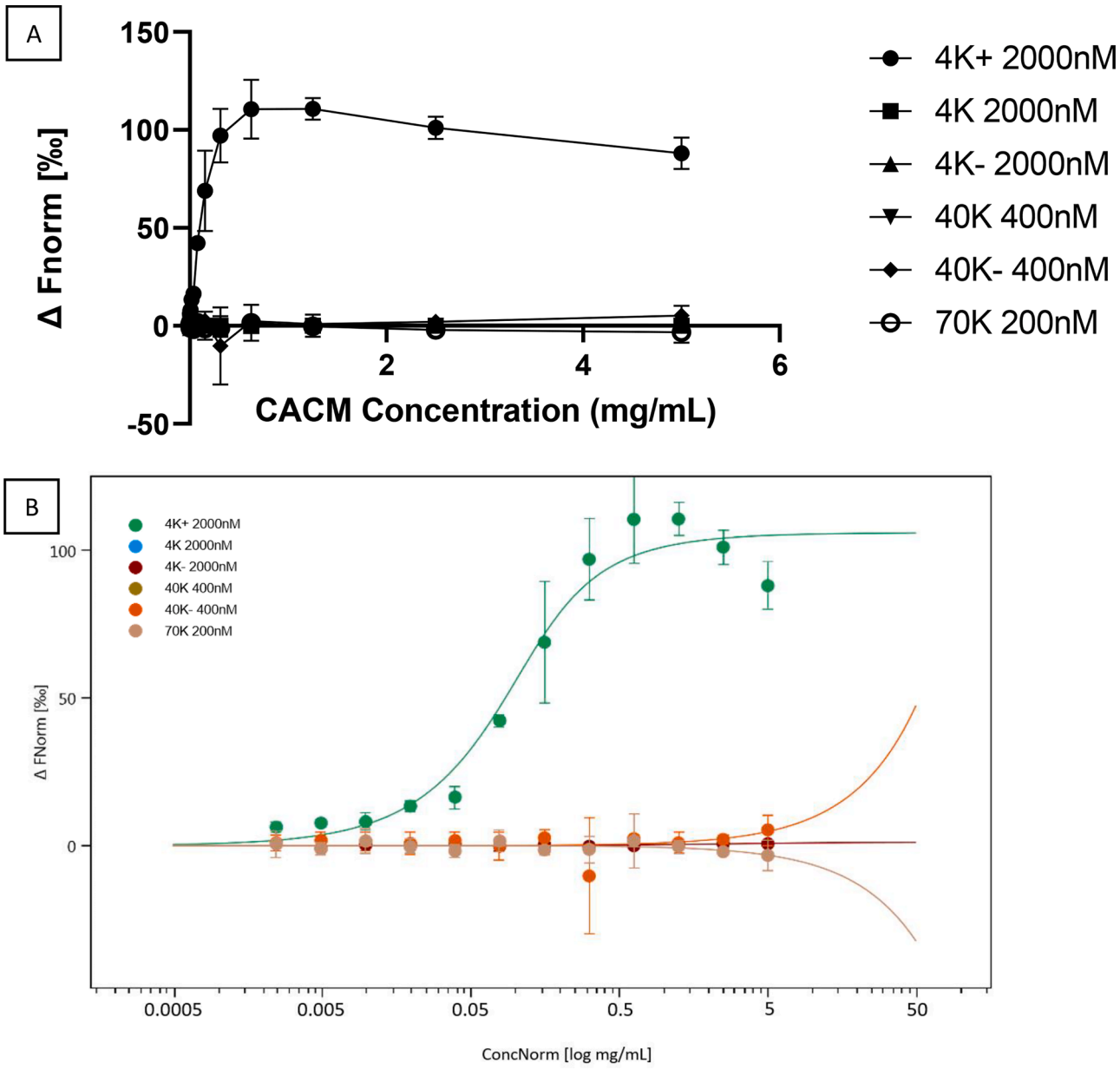

Fig. 7. Change in normalized fluorescence level indicating the binding of FITC-dextran to CACM. Negative relative fluorescence change indicates photobleaching and/or outliers in reading. Binding profile of FITC-dextrans with various charge and size properties against serial dilution of CACM (A). Fitted K_d plot of normalized fluorescence level against normalized concentration of CACM (B).

demonstrated, mucin gel assembly is regulated by synergistic effects of various contributors, such as non-mucin proteins, disulfide bridges, Ca^{2+}-mediated links, and hydrogen bonding (Meldrum et al., 2018). $CACM_{II}$ and $CACM_{III}$ samples containing 1.5 % (w/v) and 1.3 % (w/v) PAA, respectively (Fig. 2E and F), had homogenous pore networks (Fig. 2H and I), suggesting that the artificial mucus components were uniformly distributed.

Similar trends in the diffusion profiles of FITC-dextrans through colonic mucus were observed, although the diffusivity values were higher for DZ04 than DZ02 (Fig. 3A-C). In both dogs, negatively charged 4 K FITC-dextran resulted in lower mean diffusivity values than its neutral counterpart, although the difference was significant ($p < 0.001$) only for dog DZ04. The decrease could be related to potential repulsive forces between the negatively charged FITC-dextran and the negative charge of the mucus (see Table 1); (Hansing et al., 2018). In both dogs, a positive charge in the 4 K FITC-dextran resulted in significantly lower diffusivity values than for the neutral 4 K one, indicating strong electrostatic interactions between the positively charged FITC-dextran and the negatively charged mucin domains. Similar observations have been reported for pigs (Barmpatsalou et al., 2023) although the decrease was more pronounced in the dogs than pigs. This could be because the zeta potential in canine native colonic mucus (−31.6 and −32.6 for DZ02 and DZ04, respectively) is lower than in corresponding porcine mucus (ranging from −25.8 to −27.1). This would explain the stronger binding of the positively charged FITC-dextran to the negatively charged mucin domains. In both DZ02 and DZ04, the higher molecular weight FITC-dextrans (40 K and 70 K) gave significantly lower diffusivity values, compared to the 4 K one. This observation agrees with other studies reporting retardation of solute flux in the mucus (Bernkop-Schnürch and Fragner, 1996). The trend toward higher diffusivity values in DZ04 compared to DZ02 could be because of the higher water content in colonic mucus from DZ04 (94.5 %), compared to DZ02 (89.9 %) (Dubbelboer et al., 2022). Smith et al. have also found a strong correlation between water content and the diffusivity of butyrate in porcine colonic

mucus (Smith et al., 1986).

CACM captured the key diffusion patterns of FITC-dextrans in canine native colonic mucus (Fig. 4A and B). More specifically, no significant differences were observed between diffusivity values of FITC-dextrans in CACM and native colonic mucus from DZ02. Diffusion of the high molecular weight dextrans (>40 K) was slightly more restricted in CACM than in the canine native colonic mucus. This might be related to the increased rigidity of CACM due to the presence of PAA, which lacks the flexibility of native mucins, as also reported previously (Huck et al., 2019). It could also be associated with the high homogeneity of the artificial mucus network which lacks large pores. CACM followed the key trends of diffusivity profiles of FITC-dextrans in colonic mucus from dog DZ04, albeit the values were lower than in the native mucus.

In contrast to FRAP, where diffusivity is measured based on fluorescence recovery, MST provides information on the concentration dependent binding of the fluorescently labelled compound to CACM. MST is based on normalized fluorescence level under hot and cold conditions. These experiments revealed binding of cationic 4 K FITC-dextran to dispersed CACM in MES buffer. On the contrary, no binding was observed for the other studied dextrans (Fig. S5B-F). In addition, the relative fluorescence level of cationic 4 K FITC-dextran showed an increase over serial dilution of CACM, indicating hindered diffusion speed of FITC-dextran by increasing concentration of CACM in thermophoresis step (Fig.S5A). This finding can be explained by the presence of a denser CACM network in higher concentration that provides higher binding potential for the cationic 4 K FITC-dextran. Further, the lack of binding between neutral and anionic charged dextrans to CACM, regardless of the dextran size or CACM dilution, could be related to the negative charge of CACM. This finding agrees with previous studies by Rossi et al., where the authors observed that neutral or negatively charged nanoparticles are exhibiting mucopenetration properties, while positively charged particles would have mucoadhesive characteristics (Rossi et al., 2019). Additionally, the binding between CACM and cationic 4 K FITC-dextran is likely the main reason for the low diffusivity values measured for cationic 4 K FITC-dextrans in the FRAP experiment (Fig. 4); it is well-known that ionic interactions and binding greatly influence diffusion speed (Cu and Saltzman, 2009).

Although FRAP is a valuable tool for quick diffusivity measurements because it uses small sample volumes, its applicability is limited to fluorescent compounds. Therefore, the implementation of CACM in a permeation set up that enables quantification of non-fluorescent molecules was highly warranted. For this purpose, we selected the Transwell set-up that is commonly used for permeability assessments. However, in preliminary experiments, upon introduction of the donor solution on the artificial mucus, the formation of “holes” in the donor compartment was observed. Such “holes” could create a path for the diffusing molecules to directly permeate through and bypass the mucus barrier, leading to a substantial diffusion overestimation. A nylon filter was therefore carefully applied on top of the artificial mucus to ensure the formation of a homogenous mucus layer while allowing free diffusion of FITC-dextrans solution due to the large pore size (11 μm) (Alvebratt et al., 2018).

The comparison of CACM with canine native colonic mucus confirmed its ability to capture key diffusion patterns of FITC-dextrans. We therefore used the mucus model to explore drug diffusion in mucus with altered rheological properties associated with various disease conditions. The viscoelastic function of mucus is highly dependent on adequate glycosylation, sulfation, and sialylation of mucins (Smirnova et al., 2000) (Sun et al., 2016). In conditions like ulcerative colitis, sulfation of mucin decreases, which is associated with decreased viscosity and increased susceptibility to erosion and colonic inflammation (Strugala et al., 2008). On the other hand, conditions like cystic fibrosis are associated with mucus exhibiting higher viscosity than in the healthy state (Hill et al., 2018) (Button et al., 2012).

Diffusion profiles of FITC-dextrans in mucus with altered rheological properties were assayed: CACM with 0.6 % (w/v) PAA (i.e., L-CACM) and CACM with 1.8 % (w/v) PAA (i.e., H-CACM). The average permeated amount (%) of FITC-dextrans of various charges and sizes was higher in L-CACM, compared to reference CACM (Fig. 5). Similar observations have been reported regarding increased diffusion of cationic 4 K dextrans in mucus with decreased viscosity after treatment with choline-based ionic liquids (Peng et al., 2021). Likewise, the phenomenon has been observed for the diffusion of 4 K FITC-dextrans in rat mucus after N-acetyl-cysteine treatment, which resulted in mucus with lower viscosity (Takatsuka et al., 2006). In contrast, the average permeated amount (%) of FITC-dextrans of various charges and sizes was similar for the H-CACM and reference CACM. This could be due to the relatively low additional amount of PAA added to the H-CACM samples compared to the reference CACM, that resulted also in limited increase in the storage modulus and apparent viscosity profiles (Fig. S1). However, further addition of PAA was deemed impossible as it is cumbersome to dissolve the solids and this could have resulted in non-homogenous samples.

CACM was also used to explore which component of the mucus (mucin, BSA, lipids) dominated interactions with the diffusing FITC-dextrans. For all FITC-dextrans, the permeated amount (%) increased considerably in the absence of mucin and BSA indicating loss of key interactions without these components (Fig. 6A and B). The absence of lipids from the mucus mixture had only limited impact on the permeated amount (%) of FITC-dextrans. It has previously been shown that the presence of lipids in mucus plays a key role in the diffusion profile of lipophilic compounds but has only limited effect on the hydrophilic ones (Larhed et al., 1998).

In the absence of mucin and BSA, the permeated amount (%) of all FITC-dextrans increased, suggesting that they interact with both mucin and BSA, a phenomenon that results in delayed diffusion. It should be noted that the positively charged 4 K FITC-dextran had significantly more interaction with mucin than BSA, while the opposite applied for the negatively charged ones (Fig. 6A and B). Indeed, it has been previously demonstrated that the presence of mucin results in a greater decrease in diffusivity for cationic FITC-dextrans, compared to anionic ones (reported for 4 K, 40 K and 150 K FITC-dextrans) (Peng et al., 2021).

5. Conclusion

The present study describes the development of a canine artificial colonic mucus (CACM) model that was compared to native colonic mucus collected from two dogs from a research colony. The diffusivity values of macromolecules through colonic mucus were higher in one dog, albeit the same trends were observed for both dogs. The potential of the artificial mucus model to capture key trends in macromolecular diffusion through native canine mucus was demonstrated. CACM can be modified to reflect the rheological properties of low viscosity mucus, which is a characteristic of certain disease states and it was possible to replicate diffusion patterns described in the literature. Finally, CACM was successfully implemented in microscopic and macroscopic permeation assays, enabling the assessment of the diffusion of both fluorescent compounds available in small quantities and nonfluorescent compounds, respectively.

CRediT authorship contribution statement

V. Barmpatsalou: Conceptualization, Methodology, Investigation, Formal analysis, Data curation, Writing – original draft. **M. Tjakra:** Methodology, Investigation, Writing – review & editing. **L. Li:** Methodology, Investigation, Writing – review & editing. **I.R. Dubbelboer:** Methodology, Writing – review & editing. **E. Karlsson:** Conceptualization, Writing – review & editing. **B. Pedersen Lomstein:** Conceptualization, Writing – review & editing. **C.A.S. Bergström:** Conceptualization, Writing – review & editing, Funding acquisition.

Data availability

Data will be made available on request.

Acknowledgements

Financial support from VINNOVA (2019–00048) is kindly acknowledged. This project has been partially supported by the European Union's Horizon 2020 research and innovation program under the Marie Skłodowska-Curie grant agreement No. 956851. We are thankful to the Umeå Center for Electron Microscopy (UCEM) and the National Microscopy Infrastructure (NMI) for assisting with the Cryo-SEM analysis and Katarina Landberg from the Confocal Microscopy Platform at Swedish Agricultural University for assistance with the FRAP experiments. Prof. Per Hansson and Dr. Agnes Rodler are also acknowledged for providing access to the rheometer and for assistance with the rheological experiments, respectively. We are thankful for the training and guidance by Dr. Annette Roos during the MST experiments and we would like to acknowledge the Biophysical Screening and Characterization Unit at SciLifeLab for access to the Automated.NT instrument from the Department of Cell and Molecular Biology in Uppsala University.

Supplementary materials

Supplementary material associated with this article can be found, in the online version, at doi:10.1016/j.ejps.2024.106702.

References

Cone, R.A., 2009. Barrier properties of mucus. Adv. Drug Deliv. Rev. 61, 75–85.
Taherali, F., Varum, F., Basit, A.W., 2018. A slippery slope: on the origin, role and physiology of mucus. Adv. Drug Deliv. Rev. 124, 16–33.
Johansson, M.E., et al., 2014. Bacteria penetrate the normally impenetrable inner colon mucus layer in both murine colitis models and patients with ulcerative colitis. Gut 63, 281–291.
Larhed, A.W., Artursson, P., Björk, E., 1998. The influence of intestinal mucus components on the diffusion of drugs. Pharm. Res. 15, 66–71.
Bansil, R., Turner, B.S., 2006. Mucin structure, aggregation, physiological functions and biomedical applications. Curr. Opin. Colloid Interface Sci. 11, 164–170.
Dubbelboer, I.R., et al., 2022. Gastrointestinal mucus in dog: physiological characteristics, composition, and structural properties. Eur. J. Pharm. Biopharm. 173, 92–102.
Johansson, M.E., Sjövall, H., Hansson, G.C., 2013. The gastrointestinal mucus system in health and disease. Nat. Rev. Gastroenterol. Hepatol. 10, 352–361.
Boegh, M., Nielsen, H.M., 2015. Mucus as a barrier to drug delivery – understanding and mimicking the barrier properties. Basic Clin. Pharmacol. Toxicol. 116, 179–186.
Wagner, C.E., Wheeler, K.M., Ribbeck, K., 2018. Mucins and Their Role in Shaping the Functions of Mucus Barriers. Annu. Rev. Cell Dev. Biol. 34, 189–215.
Ensign, L.M., et al., 2013. Ex Vivo characterization of particle transport in mucus secretions coating freshly excised mucosal tissues. Mol. Pharm. 10, 2176–2182.
Sigurdsson, H.H., Kirch, J., Lehr, C.M., 2013. Mucus as a barrier to lipophilic drugs. Int. J. Pharm. 453, 56–64.
Bhat, P.G., Flanagan, D.R., Donovan, M.D., 1996. Drug binding to gastric mucus glycoproteins. Int. J. Pharm. 134, 15–25.
Etienne-Mesmin, L., et al., 2019. Experimental models to study intestinal microbes-mucus interactions in health and disease. FEMS Microbiol. Rev. 43, 457–489.
Sutton, S.C., 2004. Companion animal physiology and dosage form performance. Adv. Drug Deliv. Rev. 56, 1383–1398.
Sjögren, E., et al., 2014. In vivo methods for drug absorption - comparative physiologies, model selection, correlations with in vitro methods (IVIVC), and applications for formulation/API/excipient characterization including food effects. Eur. J. Pharm. Sci. 57, 99–151.
Dressman, J.B., 1986. Comparison of canine and human gastrointestinal physiology. Pharm. Res. 3, 123–131.
Dahlgren, D., et al., 2016. Regional intestinal permeability in dogs: biopharmaceutical aspects for development of oral modified-release dosage forms. Mol. Pharm. 13, 3022–3033.
Akimoto, M., et al., 2000. Gastric pH profiles of beagle dogs and their use as an alternative to human testing. Eur. J. Pharmaceutic. Biopharmac.: Off. J. Arbeitsgemeinschaft fur Pharmazeutische Verfahrenstechnik 49, 99–102. *e.V.*
Sutton, S.C., Evans, L.A., Fortner, J.H., McCarthy, J.M., Sweeney, K., 2006. Dog colonoscopy model for predicting human colon absorption. Pharm. Res. 23, 1554–1563.
Tajiri, S., et al., 2010. Colonoscopic method for estimating the colonic absorption of extended-release dosage forms in dogs. Eur. J. Pharmac. Biopharmac.: Off. J. Arbeitsgemeinschaft fur Pharmazeutische Verfahrenstechnik e.V 75, 238–244.
Wu, Y., et al., 2004. The role of biopharmaceutics in the development of a clinical nanoparticle formulation of MK-0869: a Beagle dog model predicts improved bioavailability and diminished food effect on absorption in human. Int. J. Pharm. 285, 135–146.
Deschamps, C., et al., 2022. In vitro models of the canine digestive tract as an alternative to in vivo assays: advances and current challenges. ALTEXALTEX 39, 235–257.
Tannenbaum, J., Bennett, B.T., 2015. Russell and Burch's 3Rs then and now: the need for clarity in definition and purpose. J. Am. Assoc. Lab. Animal Sci.: JAALAS 54, 120–132.
Lock, J.Y., Carlson, T.L., Carrier, R.L., 2018. Mucus models to evaluate the diffusion of drugs and particles. Adv. Drug Deliv. Rev. 124, 34–49.
Berben, P., et al., 2018. Drug permeability profiling using cell-free permeation tools: overview and applications. Eur. J. Pharm. Sci. 119, 219–233.
Fedi, A., et al., 2021. In vitro models replicating the human intestinal epithelium for absorption and metabolism studies: a systematic review. J. Controll. Rel.: Off. J. Controll. Rel. Soc. 335, 247–268.
Barmpatsalou, V., et al., 2021. Physiological properties, composition and structural profiling of porcine gastrointestinal mucus. Eur. J. Pharmac. Biopharmac.: off. J. Arbeitsgemeinschaft fur Pharmazeutische Verfahrenstechnik 169, 156–167. *e.V.*
Wikman-Larhed, A., Artursson, P., 1995. Co-cultures of human intestinal goblet (HT29-H) and absorptive (Caco-2) cells for studies of drug and peptide absorption. Eur. J. Pharm. Sci. 3, 171–183.
Béduneau, A., et al., 2014. A tunable Caco-2/HT29-MTX co-culture model mimicking variable permeabilities of the human intestine obtained by an original seeding procedure. Eur. J. Pharm. Biopharm. 87, 290–298.
Xavier, M., García-Hevia, L., Amado, I.R., Pastrana, L., Gonçalves, C., 2019. In Vitro intestinal uptake and permeability of fluorescently-labelled hyaluronic acid Nanogels. Int. J. Nanomed. 14, 9077–9088.
Kocevar-Nared, J., Kristl, J., Smid-Korbar, J., 1997. Comparative rheological investigation of crude gastric mucin and natural gastric mucus. Biomaterials 18, 677–681.
Boegh, M., Baldursdóttir, S.G., Müllertz, A., Nielsen, H.M., 2014. Property profiling of biosimilar mucus in a novel mucus-containing in vitro model for assessment of intestinal drug absorption. Eur. J. Pharmac. Biopharmac.: Off. J. Arbeitsgemeinschaft fur Pharmazeutische Verfahrenstechnik 87, 227–235. *e.V.*
Verstrepen, L., et al., 2021. Inclusion of small intestinal absorption and simulated mucosal surfaces further improve the Mucosal Simulator of the Canine Intestinal Microbial Ecosystem (M-SCIME™). Res. Vet. Sci. 140, 100–108.
Zalewsky, C.A., Moody, F.G., Allen, M., Davis, E.K., 1983. Stimulation of canine gastric mucus secretion with intraarterial acetylcholine chloride. Gastroenterology 85, 1067–1075.
Zalewsky, C.A., Moody, F.G., 1979. Mechanisms of mucus release in exposed canine gastric mucosa. Gastroenterology 77, 719–729.
Barmpatsalou, V., et al., 2023. Development and validation of a porcine artificial colonic mucus model reflecting the properties of native colonic mucus in pigs. Eur. J. Pharm. Sci. 181, 106361.
Brandl, F., et al., 2010. Hydrogel-based drug delivery systems: comparison of drug diffusivity and release kinetics. J. Controll. Rel. 142, 221–228.
Marczynski, M., et al., 2021. Structural alterations of mucins are associated with losses in functionality. Biomacromolecules 22, 1600–1613.
Patel, M.M., et al., 2003. Mucin/Poly(acrylic acid) interactions: a spectroscopic investigation of mucoadhesion. Biomacromolecules 4, 1184–1190.
Røn, T., et al., 2017. Gastric mucus and mucuslike hydrogels: thin film lubricating properties at soft interfaces. Biointerphases 12, 051001.
Falavigna, M., et al., 2018. Mucus-PVPA (mucus Phospholipid Vesicle-based Permeation Assay): an artificial permeability tool for drug screening and formulation development. Int. J. Pharm. 537, 213–222.
Lefrançois, P., et al., 2015. Insights into Carbopol gel formulations: microscopy analysis of the microstructure and the influence of polyol additives. J. Appl. Polym. Sci. 132.
Rossi, S., et al., 1995. Influence of mucin type on polymer-mucin rheological interactions. Biomaterials 16, 1073–1079.
Kim, J.-Y., Song, J.-Y., Lee, E.-J., Park, S.-K., 2003. Rheological properties and microstructures of Carbopol gel network system. Colloid Polym. Sci. 281, 614–623.
Meldrum, O.W., et al., 2018. Mucin gel assembly is controlled by a collective action of non-mucin proteins, disulfide bridges, Ca(2+)-mediated links, and hydrogen bonding. Sci. Rep. 8, 5802.
Hansing, J., Duke, J.R., Fryman, E.B., DeRouchey, J.E., Netz, R.R., 2018. Particle diffusion in polymeric hydrogels with mixed attractive and repulsive interactions. Nano Lett. 18, 5248–5256.
Bernkop-Schnürch, A., Fragner, R., 1996. Investigations into the diffusion behaviour of polypeptides in native intestinal mucus with regard to their peroral administration. Pharm. Pharmacol. Commun. 2, 361–363.
Smith, G.W., Wiggins, P.M., Lee, S.P., Tasman-Jones, C., 1986. Diffusion of butyrate through pig colonic mucus in vitro. Clin. Sci. 70, 271–276.
Huck, B.C., et al., 2019. Macro- and Microrheological properties of mucus surrogates in comparison to native intestinal and pulmonary mucus. Biomacromolecules 20, 3504–3512.
Rossi, S., et al., 2019. Recent advances in the mucus-interacting approach for vaginal drug delivery: from mucoadhesive to mucus-penetrating nanoparticles. Expert Opin. Drug Deliv. 16, 777–781.
Cu, Y., Saltzman, W.M., 2009. Mathematical modeling of molecular diffusion through mucus. Adv. Drug. Deliv. Rev. 61, 101–114.
Alvebratt, C., Cheung, O., Strømme, M., Bergström, C.A.S., 2018. A modified in situ method to determine release from a complex drug carrier in particle-rich suspensions. AAPS PharmSciTech 19, 2859–2865.

Smirnova, M.G., Birchall, J.P., Pearson, J.P., 2000. TNF-alpha in the regulation of MUC5AC secretion: some aspects of cytokine-induced mucin hypersecretion on the in vitro model. Cytokine 12, 1732–1736.
Sun, J., et al., 2016. Therapeutic potential to modify the mucus barrier in inflammatory bowel disease. Nutrients 8.
Strugala, V., Dettmar, P.W., Pearson, J.P., 2008. Thickness and continuity of the adherent colonic mucus barrier in active and quiescent ulcerative colitis and Crohn's disease. Int. J. Clin. Pract. 62, 762–769.
Hill, D.B., et al., 2018. Pathological mucus and impaired mucus clearance in cystic fibrosis patients result from increased concentration, not altered pH. Eur. Respir. J. 52, 1801297.
Button, B., et al., 2012. A Periciliary brush promotes the lung health by separating the mucus layer from airway epithelia. Science 337, 937–941.
Peng, K., et al., 2021. Modulation of gastrointestinal mucus properties with ionic liquids for drug delivery. Adv. Healthc Mater. 10, 2002192.
Takatsuka, S., Kitazawa, T., Morita, T., Horikiri, Y., Yoshino, H., 2006. Enhancement of intestinal absorption of poorly absorbed hydrophilic compounds by simultaneous use of mucolytic agent and non-ionic surfactant. Eur. J. Pharm. Biopharm. 62, 52–58.